TECHNICAL PAPER

Investigations on hardfacing and wear characteristics of nickel-based Inconel 625 overlaid welds over AISI 347 pipe

V. Rajkumar[1] · T. V. Arjunan[1] · A. Rajesh Kannan[2]

Abstract

The article focuses on investigating the effect of process parameters and wear behaviour of overlaid welds. Gas metal arc (GMAW) hardfacing is widely employed for repairing and to improve the performance of the engineering components. In this research, hardfacing is performed in the range of 130–150 A with filler wire of Inconel alloy (IN625) on the AISI 347 substrate. Successful overlaid welds were made for 150 A current at a speed of 250 mm/min and observed a continuous and even layer on the substrate. A primary current of 150 A or more can be used to overlay a uniform and continuous layer to the substrate by varying the welding speed. Higher contact angle and lower dilution were noticed at higher current and higher overlaying speeds. The increase in primary current increased the dilution and reduced the contact angle with lower bead width. In-depth microstructural examination exposed defect-free Inconel 625 hardfaced overlays with better metallurgical bonding at the interface. The overlay weld thickness varied in the range of 1.50–2.62 mm on the substrate. The hardfaced layers contain dendritic and interdendritic precipitates of Nb along the AISI 347 substrate. The intermetallic precipitates in the upper region of the overlaid weld are combined with columnar dendrites to form the Laves and (Nb, Ti) C phases. The EDS plots show the lower concentration of Fe in the IN625 overlay welds. EDS examination shows the Fe elemental dispersion and increase in the wt% of Fe in the partially melted zone of the substrate. The as-deposited overlay consists of Ni_3Si, $M_{23}C_6$ and Ni_3B phases. The micro-Vickers hardness of the hardfaced layers revealed the presence of HAZ in the substrate by GMAW process. At the applied load of 90 N, The wear rate increased with the increase in applied load on the overlaid welds from 20 to 90 N. The wear trend varies with applied load and wear time. The successfully deposited overlay welds can be suitable for worn surfaces and engineering applications to protect the stainless steels.

Keywords Inconel 625 · Hardfacing · AISI 347 · GMAW · Microstructures · Wear

1 Introduction

Surface coating processes are important as they are very useful for improving the life of worn parts by enhancing the surface properties at the worn surfaces in engineering components [1–4]. Heat exchanger components of boilers in thermal power stations, gas turbines, and food processing industries are unprotected by severe corrosive and erosive environments that lead to premature failure of the Fe-based alloy components. Several coating processes include cladding, thermal spraying, and hardfacing. The latter is an attractive option as a result of its easiness and economy [5–7]. Hardfacing is a potential overlaying process, because the coating is metallurgically bonded to the substrate and large overlay thickness can be produced than that of other coating methods like thermal spraying [8]. In this research, gas metal arc welding is used to overlay the AISI 347 pipe. However, this process doesn't require skilled welders and is economical. Although there are different types of welding processes for hardfacing, gas metal arc welding is an appropriate method because of its higher deposition rate and reliability [9, 10]. Compared to other conventional surfacing processes like galvanizing, plating, thermal spraying,

✉ V. Rajkumar
  rajkmech42@gmail.com

1 Department of Mechanical Engineering, Coimbatore Institute of Engineering and Technology, Coimbatore, Tamil Nadu 641109, India

2 Department of Mechanical Engineering, National Institute of Technology, Tiruchirappalli, Tiruchirappalli, Tamil Nadu 620015, India

etc., hardfacing has advantages such as good adhesion and adequate thickness (more than 2.5 mm from a monolayer weld) to avoid wear and/or corrosion [4]. Hardfacing is useful for treating engineering components where wear and corrosion play a key role for producing new parts, overhauling them, and enhancing the life of components in several industries [11]. Selecting appropriate materials for hardfacing on austenitic stainless steel can significantly reduce costs [12, 13]. Nickel-based alloys with higher hardness are considered for hardfacing austenitic stainless steel and have been extensively employed in repairing applications where the resistance to abrasive and impact wear is highly important [14–16]. Lower dilution ratio and improved microstructure have led the hardfacing community to employ processes such as electron beam and laser beam as a substitute for the arc welding processes. These techniques will melt the filler material together with the base metal to produce the preferred thickness over the substrate and improved metallic bonding. Even though the usage of laser or electron beam as a power source for deposition of filler wire is a favourable process, it proposes less benefits compared to gas metal arc welding (GMAW) in respect of cost saving and productivity. Austenitic stainless steels are extensively utilized in elevated temperature applications as a result of its exceptional characteristics preventing intergranular corrosion, mechanical behaviour, weldability, and economical aspects. The long-term exposure to elevated temperature environments may reduce the life of the components made of stainless steel. The overlay strength increases up to a certain limit without disturbing the base metal microstructure. One of the recognized methods for extending protection to oxidation, wear, erosion, and corrosion with low cost is the surfacing or overlaying by nickel-based superalloys on the engineering components [17, 18]. The main causes of damage are plastic deformation, wear, mechanical fatigue, and thermal fatigue [19]. Among the above types of failures, 70% of failure is due to wear [20]. Various welding processes, such as shielded metal arc welding (SMAW), oxyacetylene gas welding (OAW), submerged arc welding (SAW) and gas metal arc welding (GMAW), are frequently used to overlay hard layers. Hardfaced components must maintain their performance permanently and reliably. Hard overlays that exhibit unpredictability and excessive variability under the essential operating conditions are not used regardless of their potential benefits to the system. Hard coatings of IN 625 are currently preferred for reactor core and control rod applications where the operating temperature is between 649 and 760 °C. IN625 is also used as an overlaying material in pressure vessels due to its excellent corrosion and wear properties at elevated temperatures. Gopa et al. [21] studied the level of dilution in the base metal because of the overlaid welds which alters the microstructure and controls the wear characteristics and hardness of hard overlays. The wear characteristics and microstructural of the Ni-based overlays are superior to stainless steels [22]. The Ni-based superalloys have wide range of alloying elements than other superalloys [23]. The studies on hard overlays by Ogborn and Kotecki [24] revealed that the hard overlay microstructure was the most important factor for outstanding wear resistance. Inconel 625 (ERNiCrMo-3) is a solution-strengthened alloy, widely employed in engineering parts like turbine shrouds, aircraft duct systems, steam-line piping, chemical industry, marine components, and nuclear applications [25–27]. The metallurgical explanations on IN625 superalloys revealed the presence of γ-matrix phase in FCC lattice and secondary intermetallic phases like Ni_3Nb, FCC carbides ($M_{23}C_6$, MC, etc.), and ϒ'' Laves phase influences the properties of surfaced layers [28, 29]. In addition, his findings confirmed the Fe segregation into the solid solution of the surfaced layer and thus reduced the hardness in the IN 625 coatings. The investigations by Brussk et al. [30] on cobalt- and Ni-based superalloys revealed that IN625 achieves better oxidation resistance, erosion resistance, and wear resistance. Ahn [31] specifically classified and reviewed the surfacing methods with respect to the deposition processes. The wear performance of the hard overlays is highly relied on the surfacing alloy and the thickness of the hard deposited layers. The studies on the single-layer clad beads of IN 625 made by SMAW exhibited lower dilution at lower current level of 80 A, and resistance to wear increased under identical load conditions during wear test [32]. The mono- and multi-layer hard overlays were observed with higher dilution and reduced the wear resistance, and better resistance is observed to abrasion in the case of multiple layers [23]. Abioye et al. [33] observed that the laser-cladded IN625 microstructure on AISI 304 base metal comprises ϒ' dendritic phases, Laves phase and carbide precipitates. The studies by Gurumoorthy et al. [34] on AWS NiCr-B overlay welds over 316 LN revealed the presence of rich chromium carbides and large dendritic precipitates in the microstructure. This research brings significance to robotic hardfacing and welding in addition to wire arc additive manufacturing. Some insights into the microstructural evolution and wear characteristics of IN625 overlays have been reported.

2 Experiments and materials

2.1 Experimental system

Bead-on-pipe trials were carried out on AISI 347 pipe with IN625 filler wire using GMAW process. The diameter of the candidate pipe for overlaying was 50 mm and a thickness of 4 mm. The overlaid weld length is 100 mm. The nominal composition of the AISI 347 candidate metal and the filler wire is shown in Table 1. The overlaying

Table 1 Chemical composition (wt %) of substrate (AISI 347) and filler wire (IN625-ERNiCrMo-3)

AISI 347

Element	C	Nb	P	Si	S	Mn	Ti
wt%	0.03	0.51	0.02	0.36	0.001	1.46	0.01
Element	Cr	V	Cu	Ni	Fe	Mo	W
wt%	17.13	0.04	0.25	10.80	69.289	0.08	0.02

IN625

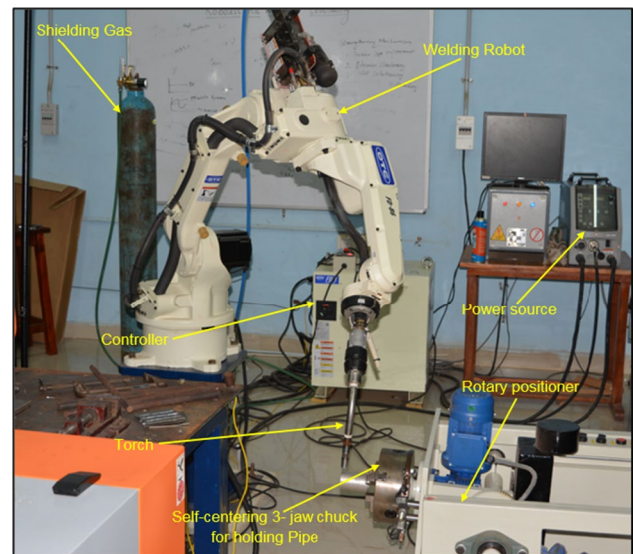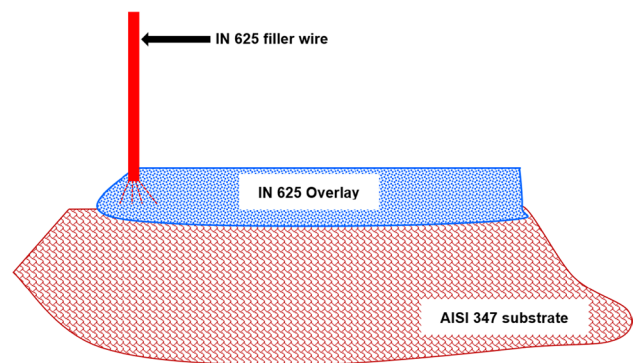| Element	Cr	P	Co	S	Si	Mn	Other
wt%	21.20	0.001	0.80	0.01	0.20	0.18	0.90
Element	Ni	Mo	Cu	C	Nb	Fe	Ti
wt%	62.20	9.20	0.25	0.05	3.80	0.8	0.4

Table 2 Input parameters for hardfacing IN625

Sample no.	Welding speed, S (mm/min)	Welding current, I (A)	Voltage, V (V)	Heat input (kJ/mm)
1	200	130	14.9	0.46
2	225	130	14.9	0.41
3	250	130	14.9	0.37
4	200	140	15.7	0.53
5	225	140	15.7	0.47
6	250	140	15.7	0.42
7	200	150	16.5	0.59
8	225	150	16.5	0.53
9	250	150	16.5	0.48

Fig. 1 Experimental setup for hardfacing IN625

parameters are depicted in Table 2. The candidate metal is mechanically grinded and cleaned with ethanol before deposition. The GMAW experimental setup including DC power source and rotary positioner is shown in Fig. 1. IN625 hard deposits were fabricated over AISI 347 pipe using a constant rate of shielding gas (98% argon + 2% CO_2). IN625 filler wire of 1.2 mm diameter is employed to deposit the hard overlays. The simplified sketch of hard surfacing process over the substrate is as shown in Fig. 2.

The welding speed of 200 mm/min, 225 mm/min, and 250 mm/min was chosen in addition to welding current of 130 A, 140 A, and 150 A in three levels to fabricate nine samples. Based on the nine trials conducted, it is confirmed that the 150 A and 250 mm/min specimen (refer to Fig. 3c) has higher thickness and lower dilution without any defects.

The welding voltage was not taken into account for hardfacing. The experimentations were made twice to ensure defect-free surfaced layers. Equation (1) is useful for calculating the heat input, Q.

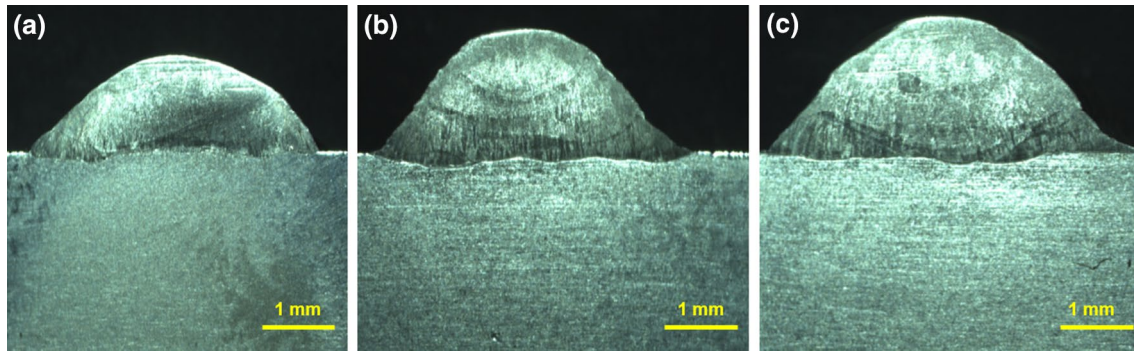**Fig. 2** Schematic sketch of IN625 hardfaced layer over substrate

Fig. 3 The overlaid weld geometry of the hardfaced with welding current. **a** 130 A—250 mm/min, **b** 140 A—250 mm/min and **c** 150 A—250 mm/min

$$Q = \frac{V * I * 60}{S * 1000} * \eta \qquad (1)$$

where V is the voltage (V), I the current (A), η the efficiency (0.8 for these trials), S the welding speed (mm/min), and Q the heat input (kJ/mm).

2.2 Metallurgical, microhardness, and wear characterization

The hardfaced specimens were cut using a wire EDM machine, grinded with various grades of SiC papers from rough to fine, and subsequently fine-polished by alumina of 1 micron. The hard deposit surface was etched with 15 mL HCl, 10 mL CH_3COOH, and 5 mL HNO_3. Macrographs and microstructural images were taken with the help of Struers welding expert and Leica metallurgical microscope. SEM–EDS is used to analyse the overlay weld composition. The overlaid weld microhardness is inspected using Vickers Microhardness Tester (Wilson Hardness 402MVD) with an applied load of 500 gf and 10 s dwell time in accordance with ASTM A264-12. The measurement was carried out in the hardfaced specimen at a distance of 0.5 mm between consecutive points. The wear characteristics (sliding) of IN625 overlaid welds were evaluated by pin-on-disc test machine following ASTM G99-17. The process parameters considered for sliding wear test are applied load, time, sliding velocity, and sliding distance [35]. The process parameters and experiment levels considered for wear test are shown in Table 3. The specimen size prepared for wear test is of 3 mm in diameter and 35 mm length. The EN8 grade steel with 35 HRC is chosen as a counterpart disc for experimentation.

The wear rate is calculated on the pin specimen using Eq. (2) [35].

$$\text{Wear rate (mm}^3\text{/m)} = \frac{(\text{Mass loss} \times \text{Density})}{\text{Sliding distance}} \qquad (2)$$

Table 3 Process parameters and experiment levels for wear test

Process parameter	Levels		
Load (N)	30	60	90
Sliding distance (m)	3000	3000	3000
Speed (rpm)	200	400	600
Sliding time (min)	90	60	30

3 Results and discussion

3.1 Effect of input parameters on hardfaced layers

The results of the visual examination confirmed the soundness of the monolayer beads made from higher heat input. Based on the trial and error responses, the width of the hardfaced layer increased as the heat input is increased [36]. For all the cases, continuity in deposition was observed while hardfacing. The spatter was low and gradually varied with respect to heat input. Figure 3 shows the macrographs of 130 A, 140 A and 150 A hardfaced layers at 250 mm/min welding speed. The bead-on-pipe experimentation clearly confirms the variation of bead width, the top reinforcement, and the dilution level of the hardfaced layers with varying heat input. The deposited layer using a welding current of 150 A and a overlaying speed range of 200–250 mm/min yielded adequate reinforcement and higher bead width was observed with less dilution. Three different combinations of heat inputs (0.48 kJ/mm, 0.53 kJ/mm, and 0.59 kJ/mm) were considered for the deposition of hard IN625 overlays after visual examination. The overlaid weld characteristics are presented in Table 4. The penetration depth (dilution) and adequate bonding depend mainly on the heat input during deposition and are calculated using Eq. 1 (refer Table 3).

From the research work by Amudha et al. [37], it is evident that higher overlay thickness can be achieved using

Table 4 Overlaid weld characteristics from experimentation results

Sample no.	Welding speed, S (mm/min)	Welding current, I (A)	Voltage, V (V)	Heat input, HI (kJ/mm)	Top reinforcement (mm)	Depth of penetration (mm)
1	200	130	14.9	0.46	1.92	0.92
2	225	130	14.9	0.41	2.06	0.78
3	250	130	14.9	0.37	2.21	0.62
4	200	140	15.7	0.53	2.54	1.67
5	225	140	15.7	0.47	2.71	1.49
6	250	140	15.7	0.42	2.96	1.32
7	200	150	16.5	0.59	3.18	2.62
8	225	150	16.5	0.53	3.35	2.37
9	250	150	16.5	0.48	3.52	2.18

hard surfacing processes. MIG-based surfacing technique was used to deposit AISI 316L over IS 2062 by Murugan et al. [38] and identified welding voltage and welding speed as the process variables considerably affect the reinforcement and dilution. The investigations by Palani et al. [39] and Balan et al. [40] highlighted the significance of using optimization techniques for cladding techniques to achieve overlay quality with lower dilution. Gunther et al. [41] employed GMAW-based hardfacing process to obtain defect-free overlay welds of FeCrC and observed welding speed and voltage as the process variables with limited experimentation. In the current research, with increasing surfacing speed from 200 to 250 mm/min, the dilution decreases and for welding current 130–150 A the top reinforcement and weld bead width increase. The studies by Kumar et al. [42] revealed the change in the overlaid bead characteristics with changing welding current and surfacing speed independently and confirmed that the heat input increased the dilution. From Fig. 3a–c it can be seen that the hardfaced sample 3 (Fig. 3a) indicates the lowest heat input per unit length as a result of the inverse relationship to the surfacing speed. When the primary current was increased beyond 150 A, the hard overlay thickness increased with higher dilution rate. The choice of surfacing speed and welding current is set to be within the limit of the maximum overlay thickness that can be achieved with a lower dilution. The primary current less than 130 A yielded lower reinforcement, and the thickness was also less.

3.2 Microstructural analysis

AISI 347 grade is a stabilized alloy with small wt% of niobium to form carbides and thereby reduces the chance of intergranular corrosion. The microstructure of sample 9 (150 A, 250 mm/min) depicting the various zones present in the overlaid weld is shown in Fig. 4. The distinct regions were observed in the hardfaced welds: a fusion zone, heat-affected zone (HAZ), partially mixed zone (PMZ), and the substrate. The diluted region is observed above the heat-affected zone and below fusion line. The base metal microstructure comprises γ-austenitic with equiaxed grains. Annealing twins are present in the austenite matrix. There is no considerable variation in the grains at the HAZ, while the dilution area is increasing from 130 to 150 A, and the lack of fusion is confirmed at lower level of welding current. There were no cracks in the overlaid welds. The overlaid weld microstructure is mainly composed of columnar dendritic structures with epitaxial growth from the base metal, identical to welding [43] for all cases.

Also, dendrite spacing and grain structure varied as the processing parameters were varied. The complete mixing is confirmed the overlaid weld where the filler metal and substrate are uniformly dispersed with even chemical composition. In the PMZ, the filler metal and substrate are bonded partially. The direction of grain growth is perpendicular to the overlaying direction as shown in Fig. 4b. The middle area depicts coarse dendrites with secondary dendritic structures. Some dendritic fragments are observed in the hardfaced micrographs. Comparable outcomes were achieved by Xu et al. [44] and Evangeline et al. [45] while overlaying IN625. This is attributed to the local temperature gradient and solidification rate during the overlaying method as the ratio of solidification rate to temperature gradient will control the grain formation after solidification [46]. A distinguishing feature of the hardfaced layer is the border which separates the partially melted and partially mixed regions [47]. Figure 4b–d relates to the hardfaced area (refer to Fig. 4b), substrate area (refer to Fig. 4c), and the interface area (refer to Fig. 4d) highlighting the heat-affected zone and unmelted zone in the hard overlay, respectively. The hardfaced area has a very fine grain dendritic structure as a result of the higher cooling rate ($G * R$) and lower G/R. In the interface area, a mixture of interdendritic and columnar structure is observed, while the substrate area has a coarse columnar dendritic structure at HAZ and well-aligned grains

Fig. 4 Microstructure of 150 A specimen at various locations. **a** IN625 hardfaced layer+substrate, **b** hardfaced layer, **c** AISI 347 substrate and **d** unmelted zone
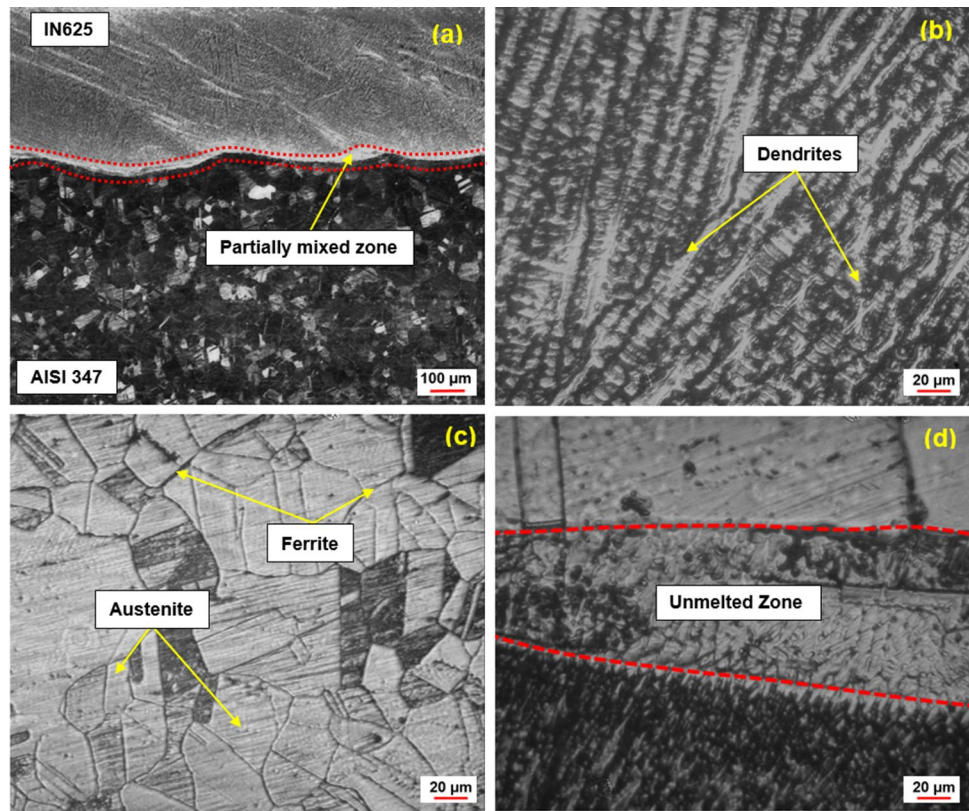
at substrate This is because the bottom area has a lower cooling rate (*G* * *R*) and a higher *G*/*R* [48]. The influence of solute and temperature gradient on the solidification front determined by the theory of constitutional supercooling outlines the dendritic solidification during overlaying [8].

3.3 EDS analysis

The base metal nominal composition is dissimilar from the filler wire used for overlaying. The unmixed region of the dissimilar overlay weld is observed in the interface between two alloys. The partly mixed zone is noticeably observed in the transverse colour etched sections of 150 A specimen as presented in Fig. 5. Also, the unmixed area separates the hardfaced layer and the substrate. EDS analysis (refer to Fig. 7) is performed for evaluating the dilution of Fe wt% in the overlaid weld. A SEM elemental mapping can be used to determine the dilution of elements [49] (refer to Fig. 9). The nominal composition examined by EDS confirms the increase in alloying elements. As observed in the melted (diluted) region in Fig. 6, the Fe wt% is 31.88 for 150 A specimen. The Fe content in the IN625 is 0.80%. This is considerably lower than the Fe wt% observed in the hard overlays by shielding metal arc welding process [32] and almost identical to laser-cladded overlays [50]. The higher Fe wt% in the diluted region reduces the resistance to corrosion [51].
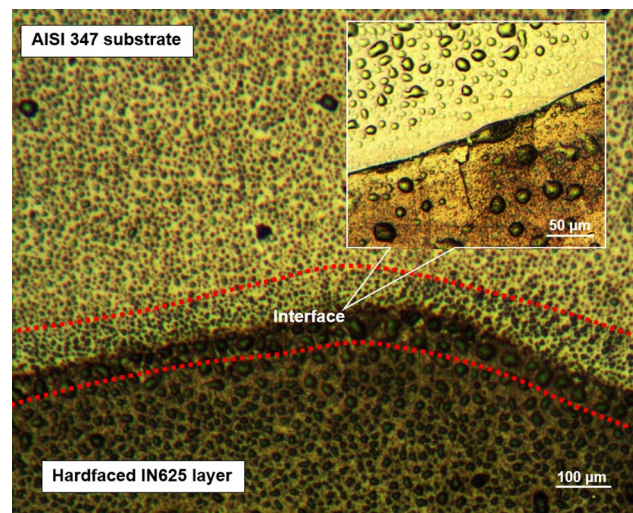

Fig. 5 Partially mixed zone micrograph of 150 A specimen

The EDS examination shows the increase in Fe dilution, when the welding current is increased. The depth of penetration is higher for 150 A overlaid weld (refer to Fig. 3c). Hence, it is confirmed that the increase in current increases the Fe wt% in the hard overlays. Also, the reduction in Nb is confirmed as the formation of NbC is observed in the hardfaced layer [29] and is evident from SEM–EDS plot shown in Fig. 7.
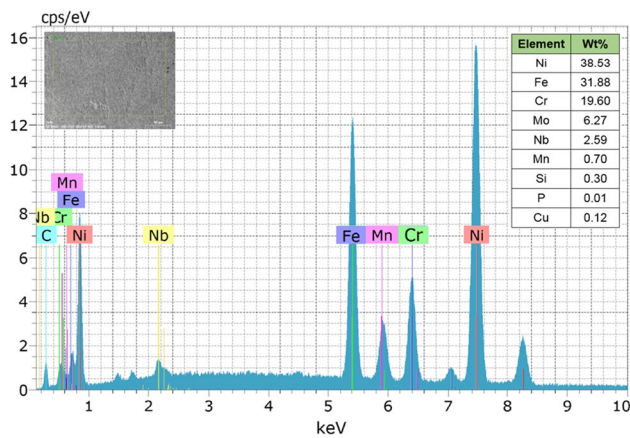
Element	Wt%
Ni	38.53
Fe	31.88
Cr	19.60
Mo	6.27
Nb	2.59
Mn	0.70
Si	0.30
P	0.01
Cu	0.12

Fig. 6 The EDS examination of Fe wt% in the melt region of the 150 A hardfaced specimen
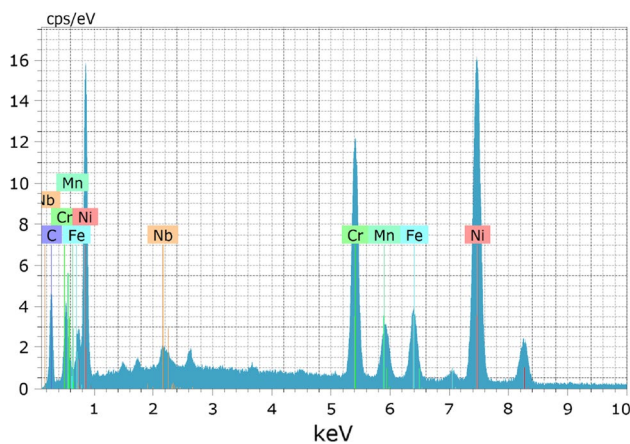

Fig. 7 The EDS examination in the IN625 hardfaced region

Figure 8 indicates the SEM micrograph of interface area in the hardfaced IN625 layer over AISI 347 revealing the dendritic structure. An EDS analysis shows the uniform dispersion of Ni, Cr, Mn, and Nb. Also, the formation of homogeneous niobium carbide (NbC) at many sites (refer to Fig. 9) was observed, resulting in the microsegregation of niobium-rich liquid bands and no solidification cracks occurred at the bonding region. From the results, it can be concluded that the temperature experienced within the range of 130–150 A is less prone to HAZ cracking in the substrate as a result of lower cooling rate. Also, reduction in the wt% of Nb confirms the formation of NbC.

3.4 Microhardness examination

Microhardness measurements were made from the hardfaced layer towards the AISI 347 of the sectioned transverse samples of the single-layer overlaid welds. Figure 10 presents the

microhardness plot of the single hardfaced layer. It confirms the higher hardness of IN625 hardfaced layer compared to interface and substrate. The composition of the substrate influences the dilution and hardness of the hardfaced layers [52]. The different areas for evaluating the hardness values are the base metal, the hardfaced layer, heat-affected zone, and the interface between overlay and substrate. The average substrate hardness is 188 HV. It is evident from the hardness graph that the hardness values trails a reducing trend from hardfaced layer (267–277 HV) towards base metal area(185–190 HV). The hardness at the interface area varied from 210 to 212 HV. The AISI 347 hardness increased noticeably in the HAZ as a result of increase in the wt% of δ-ferrite and grain growth.

The hardness results were better compared to earlier works by other researchers [51, 53]. The grain refinement in the centre of the hardfaced layers was observed with higher hardness. Identical results were reported with an increase in heat input during other surfacing methods [51].

3.5 Wear characteristics of IN625

Figure 11 shows the typical plot of wear rate in g/mm versus sliding time in minutes under various applied load of 30 N, 60 N and 90 N correspondingly. The wear trend is showing a sudden increase as the sliding time is increased from 0 to 10 min for all load conditions. As the sliding time is increased, the wear rate gradually gets stable and a sudden increase in wear is observed after a sliding time of 80 min. This phenomenon is attributed to the worn surface behaviour, i.e. the increase in wear is because of the reduction in the contact area between the friction pairs than that of the counterpart. During test, the worn surface chip off the debris in the sliding direction is highlighted in Fig. 12a–c. An increasing trend is observed for all load conditions from 30 to 90 N as the applied load is increased. The wear rate is gradually affected by the presence of Nb carbides and secondary precipitates presence in the overlaid welds. After a sliding time of 30 min, the wear rate gradually becomes steady and a minor decrease in observed in the range of 30–70 min. The secondary precipitates and carbides such as NbC and Mo_2C act as protective deposit in the hardfaced layers, and it significantly increases the wear characteristics [54].

There is only a minor difference between the wear results of 30 N and 60 N, while a major difference is there for 90 N sample. The wear rate increases as the load is doubled to 60 N, the wear loss of mass also increases in proportion. The shear stress required to separate the hard secondary phases from the base metal is insufficient at lower loads and separates these hard phases at 90 N. Figure 12 depicts the 150 A specimen worn surfaces SEM photomicrographs revealing the grooves and ploughs in the sliding direction. The wear

Fig. 8 SEM micrograph of the Inconel 625 hard overlays over AISI 347 at higher magnification (150 A sample)
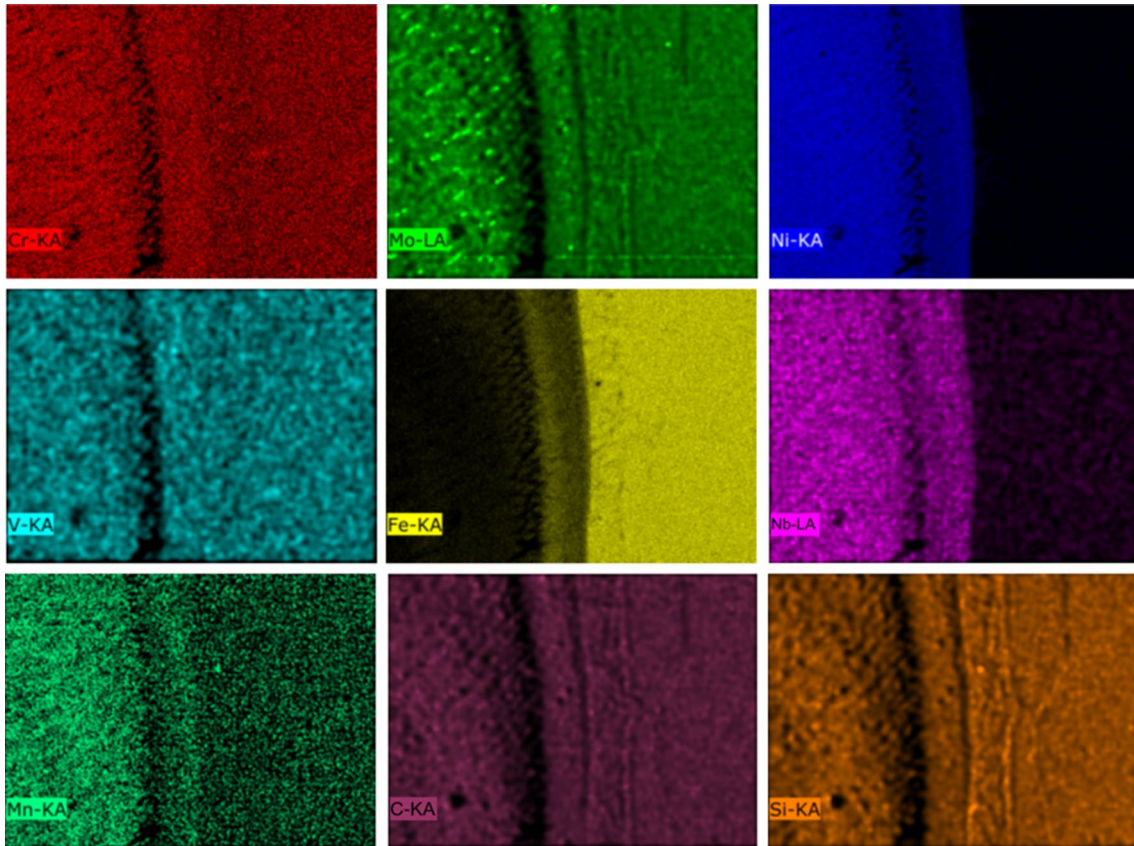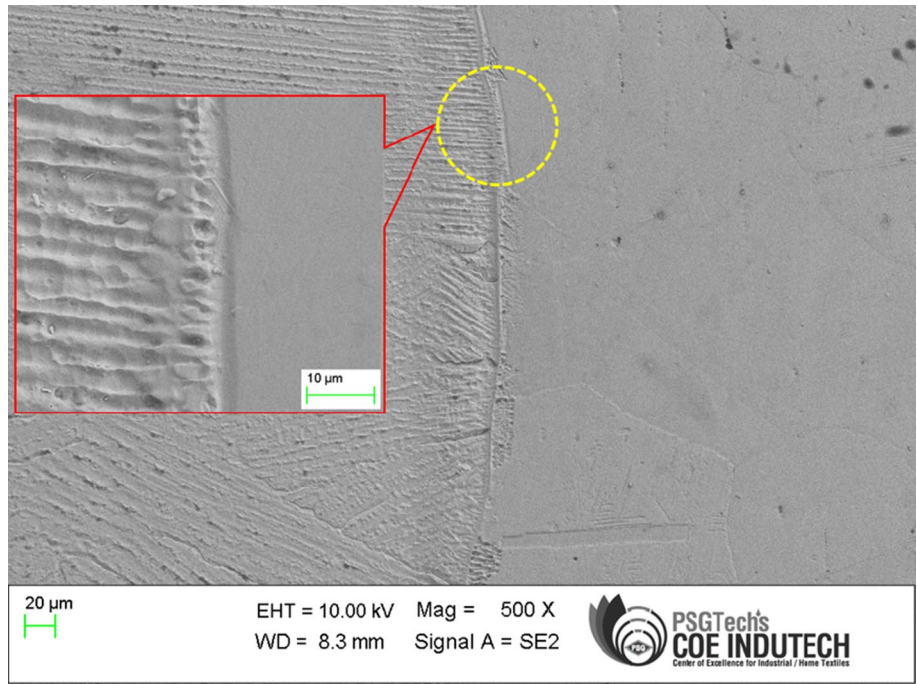

Fig. 9 Characteristic EDSX elemental mapping of the IN625 overlay highlighting the crack free in the interface (150 A sample)

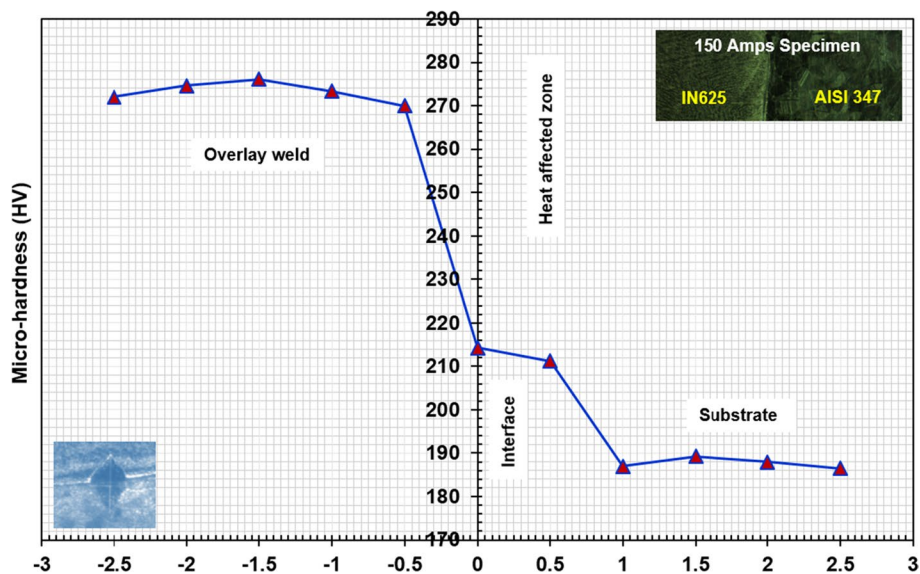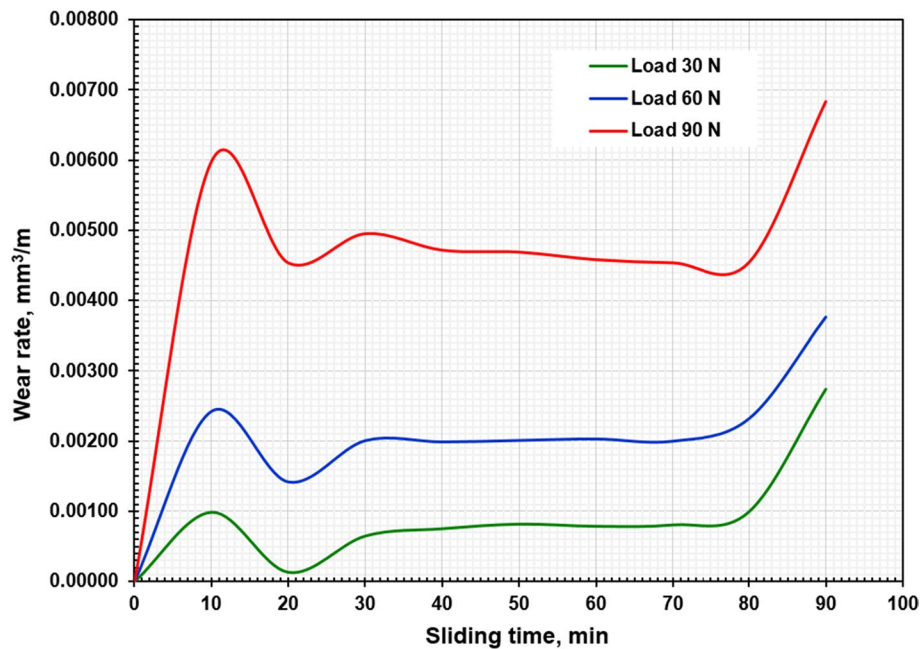**Fig. 10** Microhardness plot of 150 A overlaid specimen

Fig. 11 Typical wear rate versus sliding time of IN625 worn surface under various loads


debris formation is in the sliding direction as confirmed from the SEM micrographs [32, 55]. The formation of debris particles on the worn surface is as a result of the small chips formed initially in the hardfaced layers [45]. Ploughs and small grooves are observed during the wear test on the worn surfaces. This wear mechanism is mainly because of inherent abrasion. With the increase in sliding time, the debris size as well as the wear rate increases with the oxidation. This oxidation increased wear characteristics and alters the worn surface morphology. Wear resistance is closely related to wear properties. As the material hardness increases, the wear resistance also increases. It is confirmed that the minor difference between the hardness values of EN8 and AISI 347

is not significant, but AISI 347 has better wear resistance than EN8. This could be due to a drop in the ripple effect at a higher sliding speed, which could reduce the frictional force during wear.

4 Conclusion

The focus of this research was to assess the IN625 overlaid welds in metallurgical aspects and sliding wear behaviour in the as-deposited condition. Based on the results of this study, the following inferences were drawn:

Fig. 12 SEM micrographs of the wear track highlighting the debris formation of the worn surface
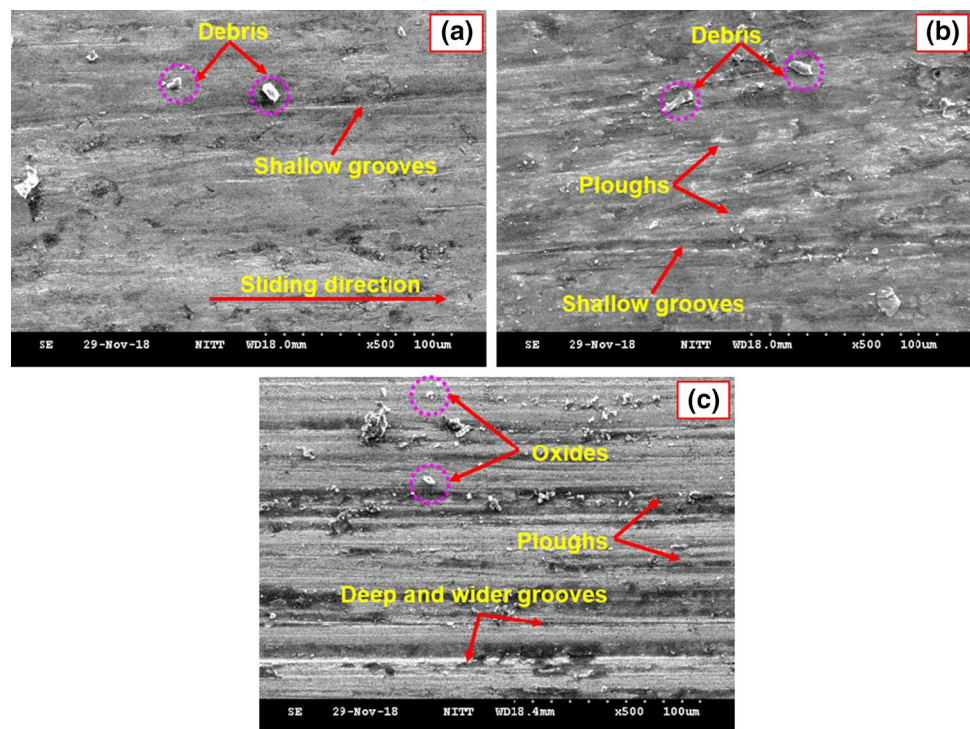
- The GMAW process can be successfully used to deposit defect-free overlay welds and is characterized by lower Fe content in the as-deposited overlays.
- Hardfaced layers did not exhibit any defects, and quality overlay welds were achieved with the following parameters: 150 A current and 250 mm/min welding speed.
- The dilution and contact angle of the overlay weld decreased beyond 150 A primary current.
- The solidified overlay welds were observed with rich dendritic cores of Ni, Cr, and Fe among the dendritic arms of Nb and Mo.
- The Fe content in the diluted region increased after weld overlaying to 31.88%.
- The overlaid weld microstructure is mainly composed of columnar dendrites. Also, dendrite spacing and grain structure varied as the processing parameters were varied.
- The micrographs reveal the presence of rich Nb and Mo phases in the interdendritic areas of the hardfaced layers.
- The SEM–EDS results highlight the variation of Fe content in the diluted region and are significantly lower in the PMZ and decrease from the interface to the top of the hardfaced deposits.
- The microhardness examination reveals a sharp drop in hardness across the interface in the hard overlay sample and reveals the presence of distinct HAZ.
- The as-deposited IN625 hard overlay constitutes Ni-rich γ (Ni, Fe) phases, carbides of $M_{23}C_6$, NbC, Ni_3Si and Ni_3B. During the 90 N load conditions, the wear trend gets high compared to 30 N and 60 N. At lower loads of 30 N abrasive-type wear is noticed, while at 90 N wear, oxidation is observed. It is evident from the pin-on-disc test that the wear mechanism differs with applied load and sliding time.
- Engineered components manufactured using stainless steels shall be protected by the IN625 hard overlays, and the multiple weld overlays can produce higher thickness on the substrate surface.

References

1. Kirchgaßner M, Badisch E, Franek F (2008) Behaviour of iron-based hardfacing alloys under abrasion and impact. Wear 265:772–779
2. Gualco Agustín, Svoboda Hernán G, Surian Estela S, de Vedia Luis A (2010) Effect of welding procedure on wear behaviour of a modified martensitic tool steel hardfacing deposit. Mater Des 31:4165–4173
3. Chatterjee S, Pal TK (2003) Wear behaviour of hardfacing deposits on cast iron. Wear 255:417–425
4. Mendez PF, Barnes N, Bell K, Borle SD, Gajapathi SS, Guest SD, Izadi H, Gola AK, Wood G (2014) Welding processes for wear resistant overlays. J Manuf Process 16:4–25
5. Zahiri R, Sundaramoorthy R, Lysz P, Subramanian C (2014) Hardfacing using ferroalloy powder mixtures by submerged arc welding. Surf Coat Technol 260:220–229
6. McPherson NA, Chi K, Baker TN (2003) Submerged arc welding of stainless steel and the challenge from the laser welding process. J Mater Process Technol 134:174–179

7. Gualco A, Svoboda HG, Surian ES (2016) Study of abrasive wear resistance of Fe-based nanostructured hardfacing. Wear 360:14–20

8. Varghese P, Vetrivendan E, Dash MK, Ningshen S, Kamaraj M, Mudali UK (2019) Weld overlay coating of Inconel 617 M on type 316 L stainless steel by cold metal transfer process. Surf Coat Technol 357:1004–1013

9. Chandel RS, Seow HP, Cheong FL (1997) Effect of increasing deposition rate on the bead geometry of submerged arc welds. J Mater Process Technol 72:124–128

10. Davis JR, Davis & Associates (1994) Stainless steel cladding and weld overlays. ASM Specialty Handbook: Stainless Steels (06398G)

11. Yang J, Yang Y, Zhou Y, Qi X, Gao Y, Ren X, Yang Q (2013) Microstructure and wear properties of Fe-2 wt% Cr-X wt% W-0.67 wt% C hardfacing layer. Weld J 92:225–230

12. Buchely MF, Gutierrez JC, Leon LM, Toro A (2005) The effect of microstructure on abrasive wear of hardfacing alloys. Wear 259:52–61

13. Balakrishnan M, Balasubramanian V, Reddy GM (2013) Effect of hardfacing consumables on ballistic performance of Q&T steel joints. Defence Technol 9:249–258

14. Coronado JJ, Caicedo HF, Gómez AL (2009) The effects of welding processes on abrasive wear resistance for hardfacing deposits. Tribol Int 42:745–749

15. Morsy M, El-Kashif E (2014) The effect of microstructure on high-stress abrasion resistance of Fe–Cr–C hardfacing deposits. Weld World 58:491–497

16. Al-fadhli HY, Stokes J, Hashmi MSJ, Yilbas BS (2006) HVOF coating of welded surfaces: Fatigue and corrosion behaviour of stainless steel coated with Inconel-625 alloy. Surf Coat Technol 200:4904–4908

17. Baldridge T, Poling G, Foroozmehr E, Kovacevic R, Metz T, Kadekar V, Gupta MC (2013) Laser cladding of Inconel 690 on Inconel 600 superalloy for corrosion protection in nuclear applications. Opt Lasers Eng 51:180–184

18. Kohopoaa J, Hakonen H, Kivivuori S (1989) Wear resistance of hot forging tools surfaced by welding. Wear 130:103–112

19. Kashani H, Amadeh A, Ghasemi HM (2007) Room and high temperature wear behaviors of nickel and cobalt base weld overlay coatings on hot forging dies. Wear 262:800–806

20. Summerville E, Venkatesan K, Subramanian C (1995) Wear processes in hot forging press tools. Mater Des 16:289–294

21. Chakraborty G, Kumar N, Das CR, Albert SK, Bhaduri AK, Dash S, Tyagi AK (2014) Study on microstructure and wear properties of different nickel base hardfacing alloys deposited on austenitic stainless steel. Surf Coat Technol 244:180–188

22. Fernandes F, Lopes B, Cavaleiro A, Ramalho A, Loureiro A (2011) Effect of arc current on microstructure and wear characteristics of a Ni-based coating deposited by PTA on gray cast iron. Surf Coat Technol 205:4094–4106

23. Charre D (1997) The microstructure of superalloys, 1st edn. Gordon and Breach Science Publishers, London

24. Kotecki DJ, Ogborn JS (1995) Abrasion resistance of iron-based hardfacing alloys. Weld J 74(8):269–288

25. UmeshBala A, Varahamoorthi R (2018) Microstructure and surface morphology characterization of laser hardfaced INCONEL-625 exposed to dry sliding wear. J Adv Microsc Res 13:239–243

26. Guoqing C, Xuesong F, Yanhui W, Shan L, Wenlong Z (2013) Microstructure and wear properties of nickel based surfacing deposited by plasma transferred arc welding. Surf Coat Technol 228:266–282

27. Hou QY, Huang ZY, Shi N, Gao JS (2009) Effects of molybdenum on the microstructure and wear resistance of nickel-based hardfacing alloys investigated using Rietveld method. J Mater Process Technol 209:2767–2772

28. Janicki D (2012) Fiber laser welding of Ni based superalloy Inconel 625. In: Proceedings of SPIE laser technology 2012: applications of lasers 8703 (2013), 87030R

29. Fesharaki MN, Shoja-Razavi R, Mansouri HA, Jamali H (2018) Microstructure investigation of Inconel 625 coating obtained by laser cladding and TIG cladding methods. Surf Coat Technol 353:25–31

30. Brussk S, Schrey A, Bamikel J, Weltersbach D, Starwald H (2014) Steam turbine valve hardfacings. Experience and latest developments. In: Proceedings of ASME turbo expo 2014: turbine technical conference and exposition, GT2014–GT26036

31. Ahn D-G (2013) Hardfacing technologies for improvement of wear characteristics of hot working tools: a review. Int J Precis Eng Manuf 14(7):1271–1283

32. Singh SS, Shahi AS (2016) Metallurgical, wear and fatigue performance of Inconel 625 weld claddings. J Mater Process Technol 233:1–8

33. Abioye TE, Folkes J, Clare AT (2013) A parametric study of Inconel 625 wire laser deposition. J Mater Process Technol 213(12):2145–2151

34. Gurumoorthy K, Kamaraj M, Prasad Rao K, Sambasiva Rao A, Venugopal S (2007) Microstructural aspects of plasma transferred arc surfaced Ni-based hardfacing alloy. Mater Sci Eng A 456(1):11–19

35. Baskaran S, Anandakrishnan V, Duraiselvam M (2014) Investigations on dry sliding wear behavior of in situ casted AA7075–TiC metal matrix composites by using Taguchi technique. Mater Des 60:184–192

36. Sowrirajan M, Koshy Mathews P, Vijayan S, Amaladasan Y (2018) Effect of weld dilution on post-weld thermal conductivity of austenitic stainless steel clad layers. Mater Res Express 5(9):096512

37. Amudha A, Shashikala HD, Nagaraja HS (2019) Corrosion protection of low-cost carbon steel with SS-309Mo and Inconel-625 bimetallic weld overlay. Mater. Res. Express 6(4):046523

38. Murugan N, Parmar RS (1994) Effects of MIG process parameters on the geometry of the bead in the automatic surfacing of stainless steel. J Mater Process Technol 41(4):381–398

39. Palani PK, Murugan N (2007) Optimization of weld bead geometry for stainless steel claddings deposited by FCAW. J Mater Process Technol 190(1):291–299

40. Balan AV, Shivasankaran N, Magibalan S (2018) Optimization of cladding parameters for resisting corrosion on low carbon steels using simulated annealing algorithm. Mater Res Express 5(4):046527

41. Günther K, Bergmann JP, Suchodoll D (2018) Hot wire-assisted gas metal arc welding of hypereutectic FeCrC hardfacing alloys: microstructure and wear properties. Surf Coat Technol 334:420–428

42. Kumar V, Lee C, Verhaeghe G, Raghunathan S (2010) CRA Weld overlay—influence of welding process and parameters on dilution and corrosion resistance. Stainless Steel World America, Toronto

43. David SA, Babu SS, Vitek JM (2003) Welding: solidification and microstructure. JOM 55(6):14–20

44. Xu X, Mi G, Chen L, Xiong L, Jiang P, Shao X, Wang C (2017) Research on microstructures and properties of Inconel 625 coatings obtained by laser cladding with wire. J Alloys Compd 715:362–373

45. Evangeline A, Sathiya P (2019) Cold metal arc transfer (CMT) metal deposition of Inconel 625 superalloy on 316 l austenitic stainless steel: microstructural evaluation, corrosion and wear resistance properties. Mater Res Express 6(6):066516

46. Kou S (2003) Welding metallurgy. Wiley, New York, pp 431–446

47. DuPont JN (1996) Solidification of an alloy 625 weld overlay. Metall Mater Trans A 27:3612–3620

48. Liu H, Li M, Qin X, Huang S, Hong F (2019) Numerical simulation and experimental analysis of wide-beam laser cladding. Int J Adv Manuf Technol 100(1):237–249

49. Abioye TE, Farayibi PK, McCartney DG, Clare AT (2016) Effect of carbide dissolution on the corrosion performance of tungsten carbide reinforced Inconel 625 wire laser coating. J Mater Process Technol 231:89–99

50. Feng Kai, Chen Yuan, Deng Pingshun, Li Yuyan, Zhao Haixing, Fenggui Lu, Li Ruifeng, Huang Jian, Li Zhuguo (2017) Improved high-temperature hardness and wear resistance of Inconel 625 coatings fabricated by laser cladding. J Mater Process Technol 243:82–91

51. Abioye T, McCartney D, Clare A (2015) Laser cladding Inconel 625 wire for corrosion protection. J Mater Process Technol 217:232–240

52. Antoszczyszyn TJ, Paes RMG, Oliveira ASCMD, Scheid A (2014) Impact of dilution on the microstructure and properties of Ni-based 625 alloy coatings. Soldag Insp 19(2):134–144

53. Silva CC, Miranda HC, Motta MF, Farias JP, Afonso CRM, Ramirez AJ (2013) New insight on the solidification path of an alloy 625 weld overlay. J Mater Res Technol 2:228–237

54. Hashim M, Babu KSR, Duraiselvam M, Natu H (2013) Improvement of wear resistance of Hastelloy C-276 through laser surface melting. Mater Des 46:546–551

55. Liu Z, Cabrero J, Niang S, Al-Taha ZY (2007) Improving corrosion and wear performance of HVOF-sprayed Inconel 625 and WC-Inconel 625 coatings by high power diode laser treatments. Surf Coat Technol 201(16):7149–7158